Brookhaven National Laboratory

BNL-227664-2025-TECH

EIC-ADD-TN-116

Study of Particle Loss in Synchrotron Phase Space Injection for ESR Using Weak-Strong Beam-Beam Simulation with Nonlinear Lattice

Y. Kan

March 2025

Electron-Ion Collider

Brookhaven National Laboratory

U.S. Department of Energy

USDOE Office of Science (SC), Nuclear Physics (NP)

DISCLAIMER

Study of Particle Loss in Synchrotron Phase Space Injection for ESR Using Weak-Strong Beam-Beam Simulation with Nonlinear Lattice

Yi-Kai Kan* and Derong Xu

Brookhaven National Laboratory, Upton, New York, USA

Abstract

In this report, we use tracking simulations to investigate synchrotron phase-space injection for electron accumulation in the electron storage ring of the Electron-Ion Collider. Our simulation model accounts for both beam-beam interactions and lattice nonlinearities. Specifically, we examine how particle loss is influenced by various parameters. Additionally, we conduct a theoretical analysis and derive an analytical formula for the rapid evaluation of particle loss. Our results demonstrate the feasibility of synchrotron phase-space injection for the electron storage ring and provide insights to guide parameter selection for the design of the injection line.

1 Introduction

The Electron-Ion Collider (EIC) consists of a hadron storage ring (HSR) of energy 41-275 GeV and the electron storage ring (ESR) of energy 5-18 GeV. In the current design, the swap-out scheme is adopted to deliver polarized electron beams to the ESR. To achieve this, a rapid cycling synchrotron (RCS) will be constructed to extract 7 nC electron bunches from the linac and boost their energy from 750 MeV to the design energy of the ESR. Recently, an upgrade path was proposed to achieve a bunch charge of 28 nC based on this scheme [1]. This plan involves building an additional beam accumulator ring (BAR) to merge four 7 nC bunches into a single bucket with 28 nC. In this study, we explore the feasibility of direct electron-accumulation in the ESR. A key

*ykan@bnl.gov

advantage of this approach is that it eliminates the need for the BAR, as bunch merging occurs directly in the ESR. However, this method may lead to emittance blow-up in the electron beam immediately after injection. A previous study on the ESR utilized both strong-strong and weak-strong simulations to investigate betatron and synchrotron phase-space injections [2]. The results showed that off-momentum deviations required by the synchrotron phase-space injection can excite synchro-betatron resonances and leads to vertical emittance blow-up. To address this, the study demonstrated that combining 200 and 400 MHz frequencies for crab cavities and reducing the longitudinal action could mitigate these effects. Consequently, the synchrotron phase-space injection was considered viable with the latest EIC design parameters. In addition to emittance control, minimizing the particle loss of injected beam is critical, as it directly impacts the injection efficiency and reduces detector background. However, the simulation model used in the earlier study approximated the entire ESR lattice with a linear one-turn map and neglected the interplay between beam-beam interactions and lattice nonlinearities. These nonlinearities could significantly contribute to particle loss. In this work, we enhance the simulation model by incorporating lattice nonlinearity to investigate the particle loss during the synchrotron phase-space injection.

To define some terminology used in our later discussion, we first give a brief introduction to the mechanism of the synchrotron phase injection. More details can be found in some literature [3, 4, 5]. The whole process of the synchrotron phase injection is illustrated in Figure 1. At the injection point (IJ) of the storage ring, the stored beam is first kicked with a distance x_{b} to a bumped orbit, where the stored beam has an acceptance $n_x^{\mathrm{s}} R_x^{\mathrm{s}}$ to the septum boundary with a chosen parameter $n_x^{\mathrm{s}} \geq 0$ (Figure 2a). Here, the notation R_x^{s} means the RMS envelope of the stored beam and is defined as

$$R_x^{\mathrm{s}} := \sqrt{(\sigma_x^{\mathrm{s}})^2 + (\eta_x^{\mathrm{s}})^2 (\sigma_\delta^{\mathrm{s}})^2} \tag{1.1}$$

with the beam size σ_x^{s}, the dispersion function η_x^{ij} at IJ and the momentum spread $\sigma_\delta^{\mathrm{s}}$. During the injection, an injected beam with an off-momentum δ_0 traverses through the injection line along an injection orbit. The injected beam also has a chosen acceptance $n_x^{\mathrm{i}} R_x^{\mathrm{i}}$ to the septum boundary; hence, one can immediately see that the separation distance between the injection orbit and the bumped orbit needs to be

$$x_0 = n_x^{\mathrm{i}} R_x^{\mathrm{i}} + S + n_x^{\mathrm{s}} R_x^{\mathrm{s}}, \tag{1.2}$$

where R_x^{i} is the RMS envelope of the injected beam, and S is the septum thickness (Figure 2b). After the injected beam passes through the injection line, the stored beam is kicked back to the closed orbit, and the injected beam is kicked to an off-momentum orbit with the separation distance x_0 to the closed orbit (Figure 2c). To have the injected beam stay on the off-momentum orbit, the dispersion function η_x^{ij} at IJ needs to satisfy

$$\delta_0 \eta_x^{\mathrm{ij}} = x_0. \tag{1.3}$$

Because higher-energy particles have stronger synchrotron radiation damping, the momentum of the injected beam will be gradually damped to the design momentum, and the off-momentum orbit will eventually merge to the closed orbit.

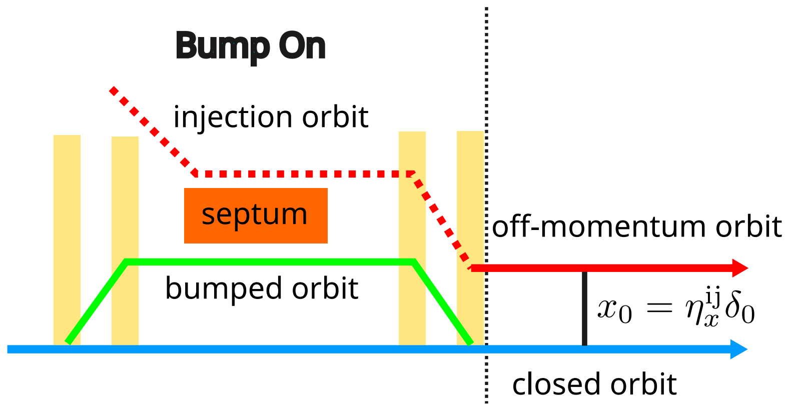

Figure 1: Schematic of the synchrotron phase-space injection

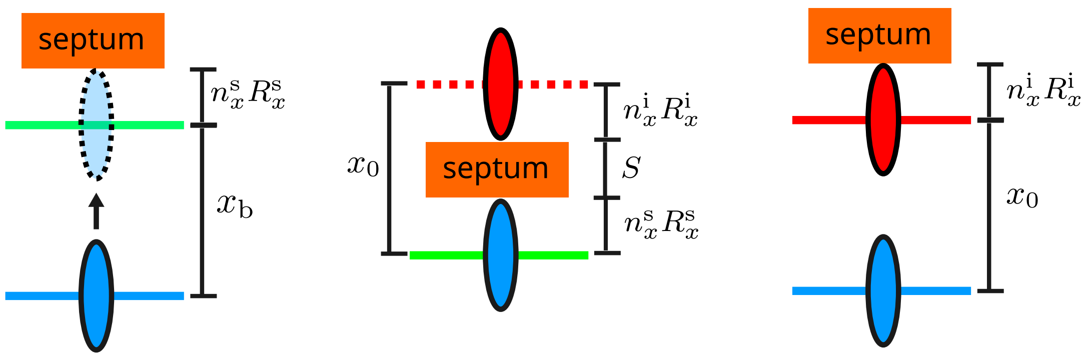

(a) before injection (b) during injection (c) after injection

Figure 2: Three stages of synchrotron phase-space injection: (a) before injection, (b) during injection and (c) after injection.

2 Weak-Strong Beam-Beam Simulation for ESR with Nonlinear Lattice

In this study, we aim to analyze the evolution of the injected beam during collider operation. To achieve this, it is essential to include the beam-beam effect in our tracking simulations in addition to the accelerator lattice. The simulations of beam-beam interaction can be classified into two approaches: weak-strong and strong-strong. In the weak-strong simulation, the particle distribution of the strong beam is assumed to remain fixed during its interaction with each test particle in the weak beam. This assumption allows the interaction force generated by the strong beam to be computed using analytical formulas. In contrast, the strong-strong model accounts for dynamic changes in the distributions of both beams during the interaction. Consequently, the electromagnetic field of the counter-propagating beam must be recalculated in real-time based on the updated particle distributions. While the strong-strong simulation captures more comprehensive physical effects (*e.g.*, coherent beam-beam effects), it comes with significantly higher computational costs due to the need to solve electromagnetic fields using the particle-in-cell method. Previous strong-strong simulations for the ESR injection of the EIC showed that the proton emittance growth rate caused by electron injection remains within an acceptable range [6, 7]. Based on these findings, our study focuses exclusively on the turn-by-turn evolution of the electron distribution, where the weak-strong model proves to be a reasonable choice for tracking simulations. This approach is particularly advantageous for modeling particle loss due to lattice nonlinearity, as the weak-strong simulation significantly reduces computational costs. Consequently, the overall simulation can be completed within a reasonable time-frame, even when lattice nonlinearity is included.

The lattice model of a storage ring typically consists of thousands of lattice elements. Tracking large amounts of particles (*e.g.,* a million particles) through each lattice element of a storage ring for several turns can be computationally demanding. To overcome this complexity, we chunk the storage ring into a few parts and use the Taylor map to approximate the corresponding transfer map for each part. One drawback of this approach is that the Taylor map is not symplectic; the symplectic error will accumulate turn by turn and eventually cause particles to be lost in long-term tracking (*e.g.,* a million turns). Fortunately, a high-energy electron storage ring has intense synchrotron radiation, and the radiation damping can mitigate the numerical growth of the symplectic error.

In our simulation model, we distinguish "kick map" and "transfer map". A kick map represents the kick at a certain location, which includes the interaction point (IP), the upstream crab cavity (UC), the downstream crab cavity (DC) or the radiofrequency cavity (RF). We denote K_i as the kick map at the location i written in small letters. Because the beam-beam interaction happens at IP, the corresponding kick map at IP is specially written as K_{bb}. A transfer map is a map between the locations of two kick maps. We write M_i^j as the transfer map from location i to location j. The position of different maps in our ESR model is illustrated in Figure 3. Therefore, at each turn, the canonical coordinates of each test particle $(x, p_x, y, p_y, z, \delta)$ will be mapped to a new set of coordinates by the composite map

$$\mathrm{D}_{\mathrm{rad}} \circ \mathrm{M}_{\mathrm{rf}}^{\mathrm{ip}} \circ \mathrm{K}_{\mathrm{rf}} \circ \mathrm{M}_{\mathrm{ip}}^{\mathrm{rf}} \circ (\mathrm{M}_{\mathrm{ip}}^{\mathrm{dc}})^{-1} \circ \mathrm{K}_{\mathrm{dc}} \circ \mathrm{M}_{\mathrm{ip}}^{\mathrm{dc}} \circ \mathrm{K}_{\mathrm{bb}} \circ \mathrm{M}_{\mathrm{uc}}^{\mathrm{ip}} \circ \mathrm{K}_{\mathrm{uc}} \circ (\mathrm{M}_{\mathrm{uc}}^{\mathrm{ip}})^{-1}, \tag{2.1}$$

where $\mathrm{D}_{\mathrm{rad}}$ is the map for the synchrotron radiation damping. The Taylor map for each transfer map in our model is calculated by Bmad [8] with the ESR lattice model (v5.6). On the other hand, the kick maps are treated separately because they mostly consist of transcendental functions and cannot be accurately approximated by the Taylor series with a finite number of terms. The details of the beam-beam kick (K_{bb}), the crab kick (K_{uc} or K_{dc}) and the radiation damping map ($\mathrm{D}_{\mathrm{rad}}$) can be found in the literature [9, 10, 2, 11, 12]. The RF kick is modeled as a single thin lens element

$$\mathrm{K}_{\mathrm{rf}} : (z, \delta) \mapsto (z, \delta + a_0 \sin(kz))$$

with a_0 the kick strength and k the wavenumber. To determine the RF kick strength a_0 and the Twiss parameters of the horizontal motion, we write down the corresponding linear one-turn map and its parametrization by the Twiss parameters

$$\overbrace{\begin{bmatrix}1 & p\\0 & 1\end{bmatrix}}^{\overline{M}^{\rm ip}_{\rm rf}[5:6,\,5:6]} \overbrace{\begin{bmatrix}1 & 0\\a_0k & 1\end{bmatrix}}^{\overline{\rm K}_{\rm rf}[5:6,\,5:6]} \overbrace{\begin{bmatrix}1 & q\\0 & 1\end{bmatrix}}^{\overline{M}^{\rm rf}_{\rm ip}[5:6,\,5:6]} = \begin{bmatrix}\cos(2\pi Q_z)+\alpha_z\sin(2\pi Q_z) & \beta_z\sin(2\pi Q_z)\\ -\gamma_z\sin(2\pi Q_z) & \cos(2\pi Q_z)-\alpha_z\sin(2\pi Q_z)\end{bmatrix}. \tag{2.2}$$

Here, we write $\overline{\rm A}$ for the linear matrix of a map A and denote $\overline{\rm A}[i{:}j,\ m{:}n]$ as the submatrix of $\overline{\rm A}$ in rows i through j and columns m through n. Solving Eq. (2.2), we can get the kick strength and the horizontal Twiss parameters

$$\mathrm{a}_0 = \frac{2(\cos(2\pi Q_z)-1)}{k(p+q)}, \alpha_z = \frac{a_0k(p-q)}{2\sin(2\pi Q_z)}, \beta_z = \frac{p+q+a_0kpq}{\sin(2\pi Q_z)}, \text{ and } \gamma_z = -\frac{a_0k}{\sin(2\pi Q_z)}. \tag{2.3}$$

Eqs. (2.3) can be readily evaluated as the values for p, q and Q_z can be computed by a lattice design program (*e.g.,* Bmad) with a lattice model.

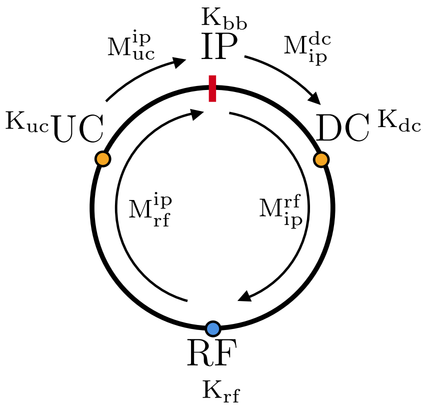

Figure 3: A schematic of the map location in the ESR ring.

We use 1.024×10^6 macro particles for the tracking of the electron beam. Some detailed simulation parameters are provided in Table 1. The turn-by-turn emittance result from our particle tracking using Taylor maps of different orders is demonstrated in Figure 4. We can observe that the emittance converges starting from the 3rd-order Taylor map. Therefore, we will use 3rd-order Taylor map for the electron injection simulation discussed in the following section. Using a 3rd-order Taylor map can also avoid the high computational cost from applying a high-order Taylor map (*e.g.,* 6th-order Taylor map).

Table 1: Simulation parameters for ESR beam-beam simulation. Parameters are mostly adapted from the EIC Conceptual Design Report [13].

Parameter	**Proton**	**Electron**
Energy (GeV)	275	10
Number of Particles per Bunch	0.688×10^{11}	1.72×10^{11}
β_x^*, β_y^* (cm)	80.0, 7.20	45.0, 5.60
ϵ_x, ϵ_y (nm · rad)	11.3, 1.00	20.0, 1.29
Bunch Length (cm)	6.0	0.7
Energy Spread	6.6×10^{-4}	5.5×10^{-4}
Q_x, Q_y (Betatron Tunes)	0.228, 0.210	0.08, 0.14
Q_z (Synchrotron Tune)	−0.010	−0.069
Crab Cavity Frequency (MHz)	200	400
Crossing Angle (mrad)	25	

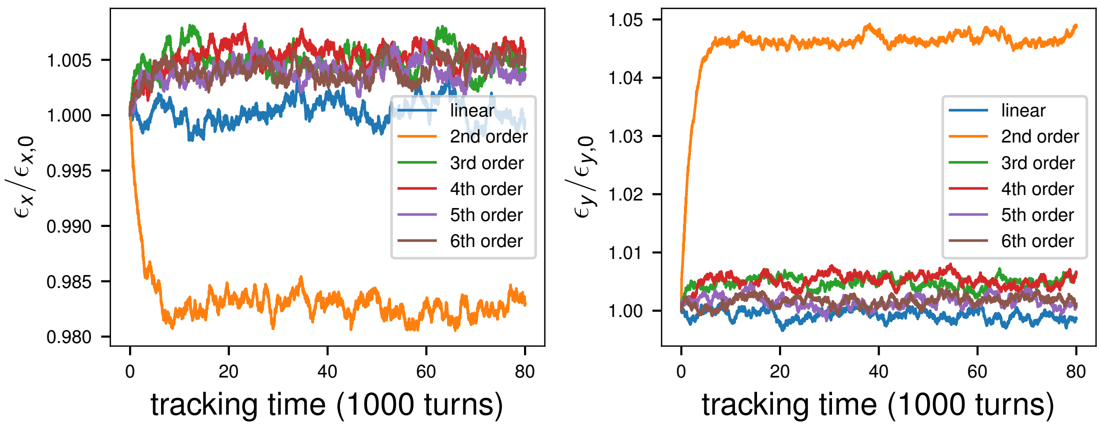

(a) without beam-beam interaction

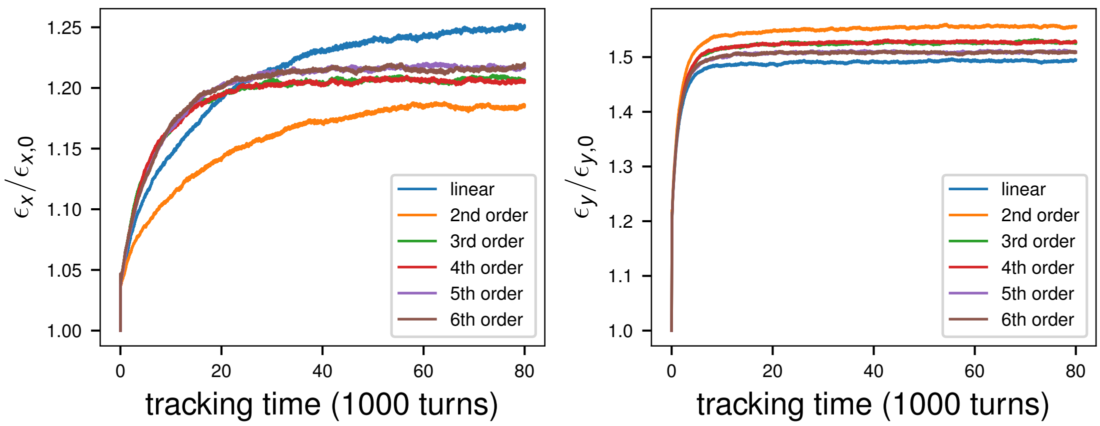

(b) with beam-beam interaction

Figure 4: The emittance from the tracking simulation for ESR using different orders of Taylor maps (a) with beam-beam interaction and (b) without beam-beam interaction. Here, $\epsilon_{x,0}$ and $\epsilon_{y,0}$ denote the initial horizontal emittance and the initial vertical emittance, respectively

3 Simulation for ESR Synchrotron Phase-Space Injection

Our injection simulation starts by generating the initial distribution of the injected beam. Each injected particle is described by the canonical coordinates $(x^{\mathrm{i}}, p_x^{\mathrm{i}}, y^{\mathrm{i}}, p_y^{\mathrm{i}}, z^{\mathrm{i}}, \delta^{\mathrm{i}})$ in the reference frame of the injected beam. After passing through the injection line, the coordinate of each injected particle becomes

$$(x^{\mathrm{i}} + \eta_x^{\mathrm{i}}\delta^{\mathrm{i}}, p_x^{\mathrm{i}}, y^{\mathrm{i}}, p_y^{\mathrm{i}}, z^{\mathrm{i}}, \delta^{\mathrm{i}}) \tag{3.1}$$

with η_x^{i} the horizontal dispersion of the injection line. To track the injected particles in the ESR lattice, a transformation of the reference frame from the injected beam to the stored beam is necessary. We use $(x^{\mathrm{ij}}, p_x^{\mathrm{ij}}, y^{\mathrm{ij}}, p_y^{\mathrm{ij}}, z^{\mathrm{ij}}, \delta^{\mathrm{ij}})$ to denote the canonical coordinates of an injected particle at IJ in the frame of the stored beam. Because the injected beam has a separation distance x_0 (Eq. (1.2)) and a momentum deviation δ_0 from the stored beam, we have the transformation below

$$\begin{aligned}
x^{\mathrm{ij}} &= x_0 + x^{\mathrm{i}} + \eta_x^{\mathrm{i}}\delta^{\mathrm{i}},\\
p_x^{\mathrm{ij}} &= (1+\delta_0)p_x^{\mathrm{i}},\\
y^{\mathrm{ij}} &= y^{\mathrm{i}},\\
p_y^{\mathrm{ij}} &= (1+\delta_0)p_y^{\mathrm{i}},\\
z^{\mathrm{ij}} &= z^{\mathrm{i}},\\
\delta^{\mathrm{ij}} &= \delta_0 + \delta^{\mathrm{i}} + \delta_0\delta^{\mathrm{i}}.
\end{aligned} \tag{3.2}$$

Here, we define $\delta_0 := (\Delta P_0 - P_0^{\mathrm{s}})/P_0^{\mathrm{s}}$ and $\Delta P_0 := P_0^{\mathrm{i}} - P_0^{\mathrm{s}}$ with P_0^{i} and P_0^{s} denoting the momenta of the injected beam and the stored beam, respectively. Because the particle tracking in each turn begins from IP (Eq. (2.1)), the injected particles need to be transferred from IJ to IP before the tracking simulation. This can be accomplished by the transfer map for the betatron motion between two locations in the accelerator line [14]. At the time of this study, we have no information about the injection line; thus, for the sake of simplicity, we make a few assumptions about the lattice at IJ:

- The Twiss function for the vertical motion is identical to that at IP.
- The horizontal alpha function at IJ is $\alpha_x^{\mathrm{ij}} = 0$.
- The phase advance from IP to IJ is 2π.

Therefore, the transfer map from IJ to IP can be written as

$$\begin{pmatrix} x^{\mathrm{ip}} \\ p_x^{\mathrm{ip}} \end{pmatrix} = \begin{pmatrix} \sqrt{\beta_x^{\mathrm{ip}}/\beta_x^{\mathrm{ij}}} & 0 \\ -\alpha_x^{\mathrm{ip}}/\sqrt{\beta_x^{\mathrm{ip}}\beta_x^{\mathrm{ij}}} & \sqrt{\beta_x^{\mathrm{ij}}/\beta_x^{\mathrm{ip}}} \end{pmatrix} \cdot \begin{pmatrix} x^{\mathrm{ij}} - \eta_x^{\mathrm{ij}}\delta^{\mathrm{ij}} \\ p_x^{\mathrm{ij}} \end{pmatrix} + \begin{pmatrix} \eta_x^{\mathrm{ip}}\delta^{\mathrm{ij}} \\ 0 \end{pmatrix}, \tag{3.3}$$

where η_x^{ip} and α_x^{ip} are usually negligible. Our simulation is not limited to the assumptions above, as we can always find out the corresponding transfer map either analytically or numerically whenever a lattice model is known. Combining Eq. (3.2) and Eq. (3.3), we can calculate the coordinates of injected particles at IP.

4 Simulation Results and Theoretical Analysis

Using the simulation model described earlier, we analyze the particle loss of the injected beam circulating in the ESR. Specifically, we examine how sensitive the particle loss is to different parameters. Our study starts with a set of base-case parameter values. For each test, we vary the value of a single parameter while keeping all other parameters fixed. The relationship between particle loss and the parameter being varied is shown in Figure 8. The results reveal that particle loss is most sensitive to β_x^{i}, $\sigma_\delta^{\mathrm{i}}$ and η_x^{ij}. To investigate this further, we define a model function $\mathcal{L} : \mathbb{R}^6 \to \{0, 1\}$ by

$$\mathcal{L}(x, p_x, y, p_y, z, \delta) = \begin{cases} 1 & \text{if lost,} \\ 0 & \text{if survived.} \end{cases}$$

Given the initial coordinates of a particle at the IP, the function $\mathcal{L}$ returns 1 if the particle is lost or 0 if it survives. We compute the mutual information between $\mathcal{L}$ and each variable using 2×10^6 data points. Each data point (X, Y) consists of a set of randomly generated particle coordinates

$$X = (x, p_x, y, p_y, z, \delta) \in \prod_k [-20\sigma_k^{\mathrm{s,ip}}, 20\sigma_k^{\mathrm{s,ip}}] \subseteq \mathbb{R}^6 \quad k \in \{x, p_x, y, p_y, z, \delta\}$$

and its corresponding "loss score" $Y \in \{1, 0\}$ computed from the beam-beam simulation. Here, the symbol $\sigma_k^{\mathrm{s,ip}}$ denotes the size of the stored beam in k-axis. The mutual information scores for $(x, p_x, y, p_y, z, \delta)$ are $(0.0924, 0.062, 0, 0, 0, 0)$. This indicates that x and p_x are the most important features influencing particle loss. Therefore, we examine the initial distribution of the injected particles at IP and project it onto the x–p_x plane (Figure 5). For the following discussion, we use the base-case parameters values listed in Table 2. From the initial distribution of the lost particles (Figure 5b), we observe that a particle is lost during the simulation if its initial $|x|$ exceeds a certain threshold. This occurs because the coordinate x of the particle lies outside the dynamic aperture Figure 6.

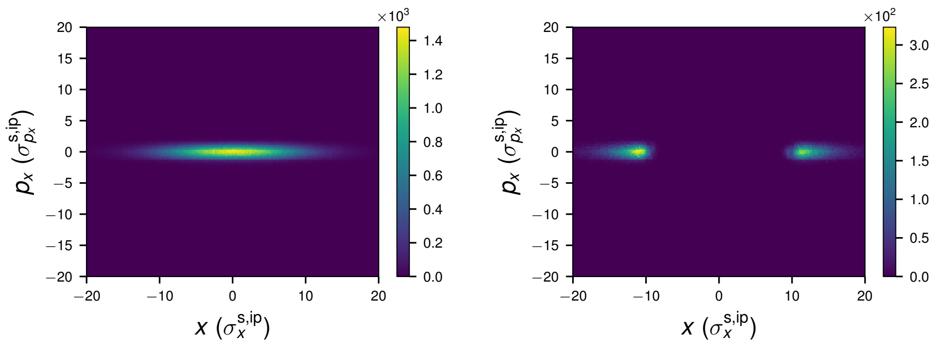

(a) all particles (b) lost particles

Figure 5: The initial particle distribution of the injected beam at IP. Figure 5a and Figure 5b show the distributions of all particles and the lost particles, respectively.

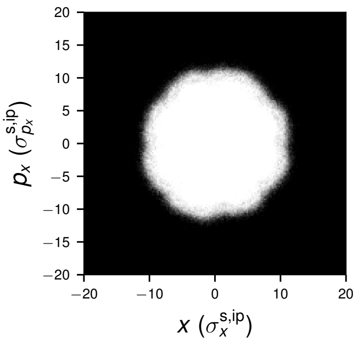

Figure 6: The dynamic aperture (white region) of ESR computed by our beam-beam simulation model. The data points are uniformly sampled on the x–p_x plane (the values for the rest of coordinates are all zero).

To gain further insight, we explicitly write out Eq. (3.3) by substituting Eq. (3.2) into Eq. (3.3) with $\eta_x^{\mathrm{ip}} = 0$ and $\alpha_x^{\mathrm{ip}} = 0$:

$$\begin{aligned} x^{\mathrm{ip}} &= \sqrt{\beta_x^{\mathrm{ip}}/\beta_x^{\mathrm{ij}}} \cdot \left(x^{\mathrm{i}} + [\eta_x^{\mathrm{i}} - \eta_x^{\mathrm{ij}}(1+\delta_0)] \cdot \delta^{\mathrm{i}} \right), \\ p_x^{\mathrm{ip}} &= \sqrt{\beta_x^{\mathrm{ij}}/\beta_x^{\mathrm{ip}}} \cdot (1+\delta_0) p_x^{\mathrm{i}}. \end{aligned} \tag{4.1}$$

If x^{i}, p_x^{i} and δ^{i} are normally distributed and mutually independent random variables, we can calculate the size of the injected beam at IP by

$$\begin{aligned} \sigma_x^{\mathrm{i,ip}} &= \mathcal{F}_x \sigma_x^{\mathrm{i}}, \\ \sigma_{p_x}^{\mathrm{i,ip}} &= \mathcal{F}_{p_x} \sigma_{p_x}^{\mathrm{i}}, \end{aligned} \tag{4.2}$$

with

$$\begin{aligned} \mathcal{F}_x &:= \sqrt{\beta_x^{\mathrm{ip}}/\beta_x^{\mathrm{ij}}} \cdot \sqrt{1 + [\eta_x^{\mathrm{i}} - \eta_x^{\mathrm{ij}}(1+\delta_0)]^2 \cdot (\sigma_\delta^{\mathrm{i}}/\sigma_x^{\mathrm{i}})^2}, \\ \mathcal{F}_{p_x} &:= \sqrt{\beta_x^{\mathrm{ij}}/\beta_x^{\mathrm{ip}}} \cdot (1+\delta_0). \end{aligned} \tag{4.3}$$

Here, σ_x^{i} and $\sigma_{p_x}^{\mathrm{i}}$ represent the sizes of the injected beam in x and p_x before passing through the injection line. From Eqs. (4.2) and Eqs. (4.3), we can clearly see why particle loss is sensitive to β_x^{i}, $\sigma_\delta^{\mathrm{i}}$ or η_x^{ij}. This is because β_x^{i} determines the value of σ_x^{i}, while $\sigma_\delta^{\mathrm{i}}$ and η_x^{ij} influence the magnitude of the stretch factor $\mathcal{F}_x$. The distribution of the injected beam is stretched in both the x and p_x axes, and the stretched beam size exceeds the dynamic aperture in the x-axis (Figure 7).

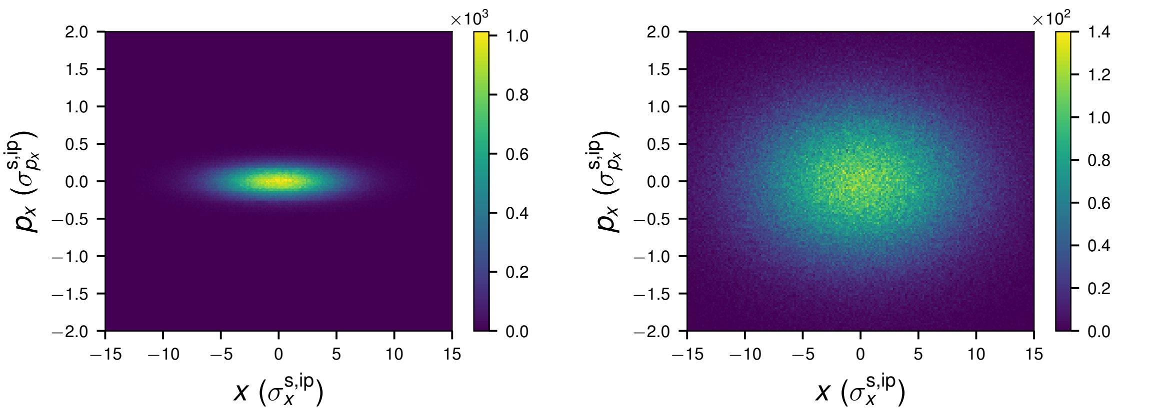

(a) the front end of the injection line (b) IP

Figure 7: The distribution of the injected beam at (a) the front end of the injection line and (b) IP.

Furthermore, using Eq. (4.2) and the region of the dynamic aperture in Figure 6, we can estimate the fraction of particle loss for the injected beam as follow

$$\mathrm{Loss} = 1 - \frac{1}{2\pi\sigma_x^{\mathrm{i,ip}}\sigma_{p_x}^{\mathrm{i,ip}}} \iint\limits_{(x/\sigma_x^{\mathrm{s,ip}})^2+(p_x/\sigma_{p_x}^{\mathrm{s,ip}})^2\leq L^2} \exp\left(-\frac{x^2}{2(\sigma_x^{\mathrm{i,ip}})^2} - \frac{p_x^2}{2(\sigma_{p_x}^{\mathrm{i,ip}})^2}\right) dx dp_x \tag{4.4}$$

with $L = 10$. Applying the formulas in [15], Eq. (4.4) can be evaluated analytically as

$$\mathrm{Loss} = \exp\left(-\frac{a^2+b^2}{4}\right)\left[I_0\left(\frac{a^2-b^2}{4}\right) + 2\sum_{n=1}^{\infty}\left(\frac{a-b}{a+b}\right) I_n\left(\frac{a^2-b^2}{4}\right)\right], \tag{4.5}$$

where we define two auxiliary variables $a := L\sigma_x^{\mathrm{s,ip}}/\sigma_x^{\mathrm{i,ip}}$ and $b := L\sigma_{p_x}^{\mathrm{s,ip}}/\sigma_{p_x}^{\mathrm{i,ip}}$, and $I_n(\cdot)$ denotes n-th order modified Bessel function of the first kind. Comparisons between the theory and the simulation is shown in Figure 9. We can see that our theory agrees well with the results from the simulation. Therefore, Eq. (4.5) can be used to quickly calculate the particle loss for an injected electron beam without performing beam-beam simulations.

5 Summary and Outlook

This study investigates synchrotron phase injection into the ESR using a weak-strong beam-beam simulation with a nonlinear lattice model. Our simulation results indicate that injecting electron beams directly into the ESR with an offset in synchrotron phase-space is feasible. Additionally, we perform a theoretical analysis to explain why certain parameters significantly influence particle loss. Furthermore, we derive a formula for the rapid evaluation of particle loss, and the theory agrees well with the results from simulations. Our findings can offer guidance for optimizing parameter selection in the design of the injection line.

Our simulation model does not account for the evolution of the proton beam distribution caused by beam-beam interactions. As shown in a previous study using strong-strong simulations [7], synchrotron phase injection into the ESR leads to a 3% emittance growth per injection in the proton beam. Exploring potential mitigation strategies for this effect is essential. Therefore, we plan to extend our model to include strong-strong beam-beam interactions.

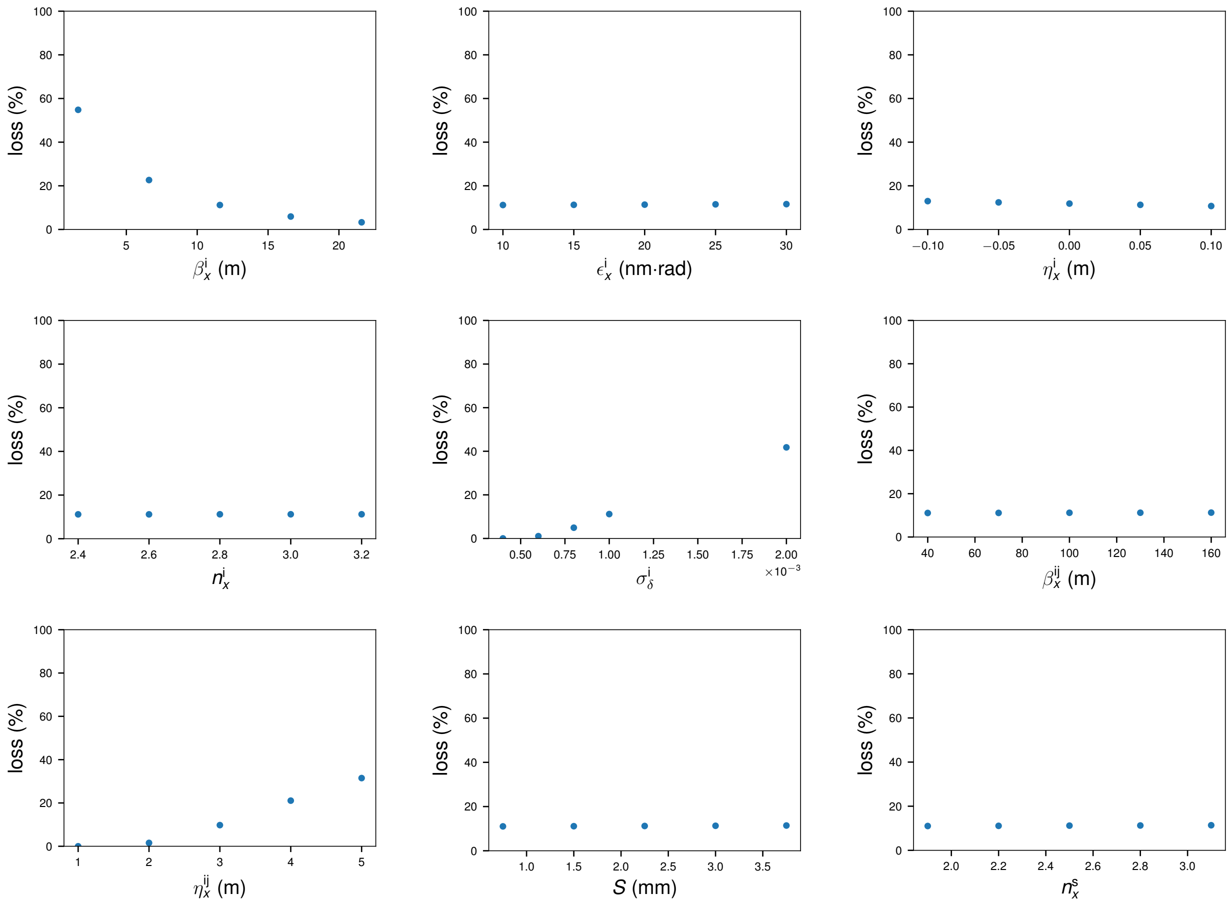

Figure 8: The the particle loss against different values of various parameters computed by our simulation model.

Table 2: The base-case parameter values for the particle loss study.

Parameter	Symbol	Value	Unit
Emittance of the Injected Beam	ϵ_x^{i}	10	nm
Beta Function of the Injection Line	β_x^{i}	11.6	m
Momentum Spread of the Injected Beam	$\sigma_\delta^{\mathrm{i}}$	1×10^{-3}	
Dispersion of the Injection Line	η_x^{i}	0.059	m
Factor Determining the Acceptance of the Injected Beam	n_x^{i}	2.8	
Beta Function at IJ of the Storage Ring	β_x^{ij}	100	m
Dispersion Function at IJ of the Storage Ring	η_x^{ij}	3.13	m
Factor Determining the Acceptance of the Stored Beam	n_x^{s}	2.5	
Septum Thickness	S	2	mm

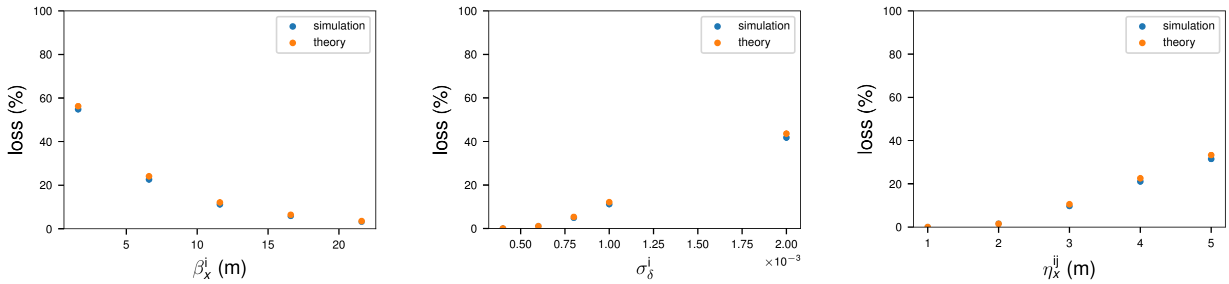

Figure 9: Comparisons between theory and simulation for particle loss versus different values of β_x^{i}, $\sigma_\delta^{\mathrm{i}}$ and η_x^{ij}.

References

[1] S. Nagaitsev, Accelerator progress, Presentation in DOE OPA CD-3B LLP Review (2025).

[2] D. Xu, Y. Hao, Y. Luo, J. Qiang, Synchrobetatron Resonance of Crab Crossing Scheme with Large Crossing Angle and Finite Bunch Length, Phys. Rev. Accel. Beams 24 (2021) 041002. doi:10.1103/PhysRevAccelBeams.24.041002.

[3] P. Collier, Synchrotron Phase Space Injection into LEP, in: Proceedings Particle Accelerator Conference, Vol. 1, 1995, pp. 551–553. doi:10.1109/PAC.1995.504716.

[4] M. Aiba, Injection: Electron Beams, CERN Yellow Rep. School Proc. 5 (2018) 121. doi:10.23730/CYRSP-2018-005.121.

[5] M. Aiba, Review of Top-up Injection Schemes for Electron Storage Rings, in: 9th International Particle Accelerator Conference, 2018. doi:10.18429/JACoW-IPAC2018-WEXGBE1.

[6] J. Qiang, et al., Transient Beam-Beam Effect During Electron Bunch Replacement in the EIC, in: Proc. IPAC'21, pp. 3228–3231. doi:10.18429/JACoW-IPAC2021-WEPAB252.

[7] D. Xu, C. Montag, F. Willeke, M. M. Blaskiewicz, Y. Luo, Advancing Electron Injection Dynamics and Mitigation Approaches in the Electron-Ion Collider's Swap-Out Injection Scheme, in: Proc. IPAC'24, no. 15, 2024, pp. 230–233. doi:10.18429/JACoW-IPAC2024-MOPC72.

[8] D. Sagan, Bmad: A Relativistic Charged Particle Simulation Library, Nucl. Instrum. Meth. A558 (1) (2006) 356–359, proceedings of the 8th International Computational Accelerator Physics Conference. doi:https://doi.org/10.1016/j.nima.2005.11.001.

[9] K. Hirata, H. W. Moshammer, F. Ruggiero, A Symplectic Beam-Beam Interaction with Energy Change, Part. Accel. 40 (1993) 205–228.
URL https://cds.cern.ch/record/243013

[10] K. Hirata, Analysis of Beam-Beam Interactions with a Large Crossing Angle, Phys. Rev. Lett. 74 (1995) 2228–2231. doi:10.1103/PhysRevLett.74.2228.

[11] D. Xu, V. S. Morozov, D. Sagan, Y. Hao, Y. Luo, Enhanced Beam-Beam Modeling to Include Longitudinal Variation During Weak-Strong Simulation, Phys. Rev. Accel. Beams 27 (2024) 061002. doi:10.1103/PhysRevAccelBeams.27.061002.

[12] J. Qiang, M. A. Furman, R. D. Ryne, Strong-Strong Beam-Beam Simulation using a Green Function Approach, Phys. Rev. ST Accel. Beams 5 (2002) 104402. doi:10.1103/PhysRevSTAB.5.104402.

[13] F. Willeke, J. Beebe-Wang, Electron Ion Collider Conceptual Design Report 2021, Tech. rep., Brookhaven National Lab. (BNL), Upton, NY (United States); Thomas Jefferson National Accelerator Facility (TJNAF), Newport News, VA (United States) (02 2021). doi:10.2172/1765663.

[14] S.-Y. Lee, Accelerator Physics, 4th Edition, WORLD SCIENTIFIC, 2019. doi:10.1142/11111.

[15] J. Waugh, Evaluation of Integral of Elliptical Gaussian Distribution over a Centered Ellipse, Tech. Rep. NAVNWEPS REPORT 7782, US Naval Ordnance Test Station (1961).